# Complex Impedance Transformers Based on Branch-Line Hybrid Couplers

**Pablo Alcón\*, Nuria Esparza, Luis Fernando Herrán, and Fernando Las-Heras**

**Abstract**—A topology, equations and design methodology for complex impedance-transforming branch-line hybrid couplers are presented. This method also allows the realization of real impedance-transforming to higher impedances. Limitations for real, imaginary and complex impedances are discussed. Test results are shown for a $3\,\mathrm{dB}$ 50 to $450\,\Omega$ hybrid coupler, at a $2\,\mathrm{GHz}$ center frequency, with a 21% bandwidth, an amplitude balance of $4.35 \pm 1\,\mathrm{dB}$ and a phase balance of $92.16° \pm 8.8°$. To showcase the complex impedance scenario, two $3\,\mathrm{dB}$ $50\,\Omega$ to $70 - 200j\,\Omega$ are measured at a $2\,\mathrm{GHz}$ center frequency. One of these couplers uses a technique for reducing the chip size, yielding a 22.5% bandwidth, $4 \pm 0.9\,\mathrm{dB}$ amplitude balance and $93.22° \pm 6.74°$ phase balance, while accomplishing a 25% size reduction.

## 1. INTRODUCTION

Branch line hybrid couplers are prominently used in the design of many microwave circuits (e.g., data modulators, phase shifters, balanced amplifiers and feeding networks). Most of the research on this structure focuses on achieving circuit miniaturization and bandwidth plus isolation enhancement through different techniques, including left-handed transmission lines [1], via-holes [2, 3], air-gaps [4], stubs [5, 6], coupled [7, 8] and $\pi$-shaped lines [9].

Hybrids that also transform the input impedance to a lower value are also of interest, since they significantly reduce the number of elements required in FET matching [10] and increase the performance of phase shifters [11]. Additionally, transforming to higher impedance is useful to feed antennas [12]. However, the impedance transformation is limited by the feasibility of the line impedance of the branches and reduced to real values [13]. Consequently, transforming to a high impedance requires using lines whose widths are unattainable. In other cases, a complex output impedance is needed for maximum power transfer, or for better performance in circuits such us reflective-type phase shifters without resorting to adding lumped capacitances or inductances [14], which increases complexity and cost. Nonetheless, no solutions to these problems for branch-line hybrid couplers can be found in the literature, requiring the use of external matching networks for each port, negating the possible circuit miniaturization with previous techniques by the resulting size increase that it would incur.

To overcome these limitations, this paper proposes a modification of the original topology of the impedance transforming hybrid [10] based on the possibility of matching complex impedances using transmission lines with appropriate lengths [15]. Therefore, this topology can increase the impedance transforming ratio (defined as the ratio of output/input impedance) and achieve maximum power transfer with complex impedances. Moreover, it can also be used to reduce the line width when transforming to a lower impedance, and to scale down the line length of the transformer, enabling a reduction of the chip size.

An analysis of the circuit is presented, and two different impedance transforming hybrids from $50\,\Omega$ to $70 - 200j\,\Omega$ are designed, simulated, manufactured and measured to validate its performance and the small-scale impact of reducing the line length for matching $50\,\Omega$.

## 2. ANALYSIS AND DESIGN

The proposed circuit consists in a modification of the original impedance transforming hybrid coupler, adding transmission lines of arbitrary impedances, $Z_1$ and $Z_2$, and arbitrary electrical lengths, $L_1$ and $L_2$, to each port of the regular topology (Fig. 1). These lines will transform the branch ($Z_{B1}$, $Z_{B2}$) impedances. $Z_0$ refers to the impedance in ports 1 and 2, and $Z_T$ in ports 3 and 4, which are the impedances the hybrid coupler will be transformed to.
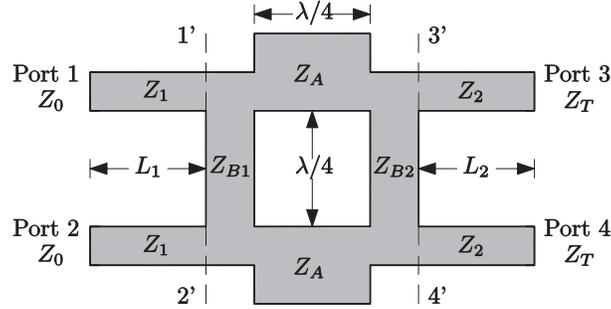


**Figure 1.** Diagram of the proposed hybrid coupler. Port locations of the original topology are marked with an apostrophe.

Due to passive and lossless conditions, the following relations between the scattering parameters are assumed:

$$|S_{11}|^2 + |S_{21}|^2 + |S_{31}|^2 + |S_{41}|^2 = 1 \tag{1}$$

$$|S_{33}|^2 + |S_{43}|^2 + |S_{31}|^2 + |S_{41}|^2 = 1 \tag{2}$$

where $S_{33} = \dfrac{Z_T{}^* - Z_0}{Z_T{}^* + Z_0}$.

Since ports 1 and 2 will be matched to the reference impedance, it is found that $|S_{11}| = 0$ and $|S_{43}| = 0$ [10]. Furthermore, the coupling factor between $S_{31}$ and $S_{41}$ is defined so $|S_{31}| = k \cdot |S_{41}|$. Applying these two conditions to Equations (1) and (2), it is obtained that

$$|S_{21}| = |S_{33}| \tag{3}$$

$$|S_{41}| = \sqrt{\frac{1 - |S_{33}|^2}{1 + k^2}} \tag{4}$$

Thus, the magnitude of the scattering parameters matrix referenced to $Z_0$ is as follows:

$$|S| = \begin{pmatrix} 0 & |S_{33}| & k \cdot \sqrt{\dfrac{1 - |S_{33}|^2}{1 + k^2}} & \sqrt{\dfrac{1 - |S_{33}|^2}{1 + k^2}} \\[4mm] |S_{33}| & 0 & \sqrt{\dfrac{1 - |S_{33}|^2}{1 + k^2}} & k \cdot \sqrt{\dfrac{1 - |S_{33}|^2}{1 + k^2}} \\[4mm] k \cdot \sqrt{\dfrac{1 - |S_{33}|^2}{1 + k^2}} & \sqrt{\dfrac{1 - |S_{33}|^2}{1 + k^2}} & |S_{33}| & 0 \\[4mm] \sqrt{\dfrac{1 - |S_{33}|^2}{1 + k^2}} & k \cdot \sqrt{\dfrac{1 - |S_{33}|^2}{1 + k^2}} & 0 & |S_{33}| \end{pmatrix} \tag{5}$$

When ports 3 and 4 are renormalized to $Z_T$, the scattering parameters end up being those of the typical hybrid coupler:

$$|S| = \begin{pmatrix} 0 & 0 & \dfrac{k}{\sqrt{1+k^2}} & \dfrac{1}{\sqrt{1+k^2}} \\[2ex] 0 & 0 & \dfrac{1}{\sqrt{1+k^2}} & \dfrac{k}{\sqrt{1+k^2}} \\[2ex] \dfrac{k}{\sqrt{1+k^2}} & \dfrac{1}{\sqrt{1+k^2}} & 0 & 0 \\[2ex] \dfrac{1}{\sqrt{1+k^2}} & \dfrac{k}{\sqrt{1+k^2}} & 0 & 0 \end{pmatrix} \tag{6}$$

Thanks to the circuit symmetry, the scattering parameters of Fig. 1 are easily obtained through an even-odd mode four-port network analysis [16]. Considering $Z_1$ and $Z_2$ as arbitrary impedances, and with the imposition of $Z_0$ and $Z_T$ as input/output impedances, the values of $Z_{B1}$, $Z_{B2}$ and $Z_A$ must be found so that the scattering parameters comply with Equation (5).

Applying isolation,

$$S_{43} = 0 \tag{7}$$

matching,

$$S_{33} = \frac{Z_T{}^* - Z_0}{Z_T{}^* + Z_0} \tag{8}$$

and coupling conditions

$$S_{31} = j \cdot k \, S_{41} \tag{9}$$

it is found that

$$Z_{B1} = k \, Z_1 \, \frac{Z_0 + j \, Z_1 \, \tan(L_1)}{Z_1 + j \, Z_0 \, \tan(L_1)} \tag{10a}$$

$$Z_{B2} = k \, Z_2 \, \frac{Z_T + j \, Z_2 \, \tan(L_2)}{Z_2 + j \, Z_T \, \tan(L_2)} \tag{10b}$$

$$Z_A = \sqrt{\frac{Z_{B1} \, Z_{B2}}{1 + k^2}} \tag{10c}$$

The electrical lengths $L_1$ and $L_2$ must comply with $Z_{B1}$ and $Z_{B2}$ being real. Thus,

$$L_1 = \arctan\left(\frac{Z_1{}^2 - |Z_0|^2 \pm \sqrt{\left(|Z_0|^2 + Z_1{}^2\right)^2 - (2 \, Z_1 \, \mathrm{Re}\{Z_0\})^2}}{2 \, Z_1 \, \mathrm{Im}\{Z_0\}}\right) + n \cdot \pi \tag{11}$$

$$L_2 = \arctan\left(\frac{Z_2{}^2 - |Z_T|^2 \pm \sqrt{\left(|Z_T|^2 + Z_2{}^2\right)^2 - (2 \, Z_2 \, \mathrm{Re}\{Z_T\})^2}}{2 \, Z_2 \, \mathrm{Im}\{Z_T\}}\right) + n \cdot \pi \tag{12}$$

where $n = \{0, 1\}$.

For each length, there are two periodic solutions with period $\pi$. Each one of these solutions produces a different branch-line impedance. Since both branch-line impedances affect $Z_A$, there will be four different set of solutions.

Therefore, every impedance is defined by the coupling factor, the port impedances, the design impedances $Z_1$ and $Z_2$, and the electrical lengths $L_1$ and $L_2$.

Observing Equations (10a) and (10b), it can be surmised that the lines at each port act as complex impedance transformers that take the branch-line impedances as loads and match them to $Z_0$ and $Z_T$.

## 2.1. Design Process

For obtaining a hybrid coupler with any values for input impedance $Z_0$, output impedance $Z_T$ and coupling factor $k$, the design process is as follows:

(i) Definition of desired lower and upper impedance limits, $Z_{min}$ and $Z_{max}$. They represent the fabrication or size limits which cannot be exceeded.

(ii) Value assignment for impedances $Z_1$ and $Z_2$.

(iii) Through Equations (11) and (12), calculation of every solution for electrical lengths $L_1$ and $L_2$.

(iv) With the different lengths, evaluation of every possible combination of $Z_{B1}$, $Z_{B2}$ and $Z_A$ (Equations (10a)–(10b)).

(v) Choosing of the combination with impedance values within limits. If there are none, return to step (ii).

$Z_1$ and $Z_2$ are the only unknowns of the design, and if a solution is achievable, finding it would depend on the right assignment of their values. Thus, reaching a solution is an iterative process that can be sped up through an optimization algorithm such as the gradient method.

## 2.2. Impedance Matching Limitations

Different impedance transformations force their own restrictions to the line impedances of the hybrid coupler.

### 2.2.1. Real Impedances

If $Z_T$ is real, the electrical length $L_2 = 90°$, so

$$Z_{B2} = k \frac{Z_2{}^2}{Z_T} \tag{13}$$

and the only limitation would be the ratio of highest to lowest possible impedance.

As an example, for $Z_0 = 50\,\Omega$, $Z_{min} = 20\,\Omega$, $Z_{max} = 150\,\Omega$, and $k = 1$, it would be impossible to achieve solutions for $Z_T$ below $3\,\Omega$ or above $1100\,\Omega$. In Table 1 it is shown that for $Z_T$ close to those values, the resulting impedances are also close to the limits.

**Table 1.** Set of solutions for matching real impedances with $Z_{min} = 20\,\Omega$, $Z_{max} = 150\,\Omega$, and $k = 1$.

| $Z_T$ | $Z_1$ | $Z_2$ | $Z_{B1}$ | $Z_{B2}$ | $Z_A$ | $L_1$ | $L_2$ |
|---|---|---|---|---|---|---|---|
| $5\,\Omega$ | $57.24\,\Omega$ | $27.05\,\Omega$ | $65.53\,\Omega$ | $146.33\,\Omega$ | $69.25\,\Omega$ | $90°$ | $90°$ |
| $1000\,\Omega$ | $89.98\,\Omega$ | $149.49\,\Omega$ | $161.94\,\Omega$ | $22.35\,\Omega$ | $42.54\,\Omega$ | $90°$ | $90°$ |

Reducing the lowest impedance to $10\,\Omega$ and increasing the highest to $200\,\Omega$ (thus increasing the aforementioned ratio) improves the capability of matching to higher and lower impedances, as demonstrated in Table 2.

**Table 2.** Set of solutions for matching real impedances with increased limits $Z_{min} = 10\,\Omega$, $Z_{max} = 200\,\Omega$, and $k = 1$.

| $Z_T$ | $Z_1$ | $Z_2$ | $Z_{B1}$ | $Z_{B2}$ | $Z_A$ | $L_1$ | $L_2$ |
|---|---|---|---|---|---|---|---|
| $1\,\Omega$ | $32.91\,\Omega$ | $12.32\,\Omega$ | $21.66\,\Omega$ | $151.79\,\Omega$ | $40.55\,\Omega$ | $90°$ | $90°$ |
| $3500\,\Omega$ | $67.33\,\Omega$ | $192.38\,\Omega$ | $90.64\,\Omega$ | $10.57\,\Omega$ | $21.89\,\Omega$ | $90°$ | $90°$ |

### 2.2.2. Imaginary Impedances

If $Z_T$ is imaginary, there are two possible lengths, resulting in two different $Z_{B2}$ impedances. On one hand:

$$L_2 = \arctan\left(\frac{j\,Z_2}{Z_T}\right) \tag{14}$$

$$Z_{B2} = k\,Z_2\,\frac{Z_T - \dfrac{Z_2{}^2}{Z_T}}{Z_2 - Z_2} = \infty \tag{15}$$

On the other:

$$L_2 = \arctan\left(\frac{j\,Z_t}{Z_2}\right) \tag{16}$$

$$Z_{B2} = k\,Z_2\,\frac{Z_T - Z_T}{Z_2 - \dfrac{Z_T{}^2}{Z_2}} = 0 \tag{17}$$

Neither of which are feasible. Consequently, imaginary impedances cannot be matched.

### 2.2.3. Complex Impedances

When the matching impedance is complex, an additional restriction is added to the case of a real impedance, which applies to the branch-line impedance of the corresponding matching port, i.e., $Z_1$ and $L_1$ for $Z_0$, and $Z_2$ and $L_2$ for $Z_T$. For instance, matching a complex $Z_T$ with $Z_2 = 100\,\Omega$ and $k = 1$ yields the results shown in Table 3.

**Table 3.** Effects of the imaginary part for matching complex impedances on the possible values of a branch-line impedance. Extra numerical suffixes indicate the two possible solutions for each case.

| $Z_T$ | $L_{2_1}$ | $Z_{B2_1}$ | $L_{2_2}$ | $Z_{B2_2}$ |
|---|---|---|---|---|
| $70 - 20j\,\Omega$ | $20.2°$ | $65.2\,\Omega$ | $290.2°$ | $153.37\,\Omega$ |
| $70 - 200j\,\Omega$ | $65.55°$ | $12.96\,\Omega$ | $335.55°$ | $771.32\,\Omega$ |
| $70 - 2000j\,\Omega$ | $87.14°$ | $0.17\,\Omega$ | $357.14°$ | $57356\,\Omega$ |

From Table 3, it can be surmised that the more the impedance $Z_T$ resembles a pure imaginary impedance (i.e., the bigger the ratio of imaginary part to real part), the higher or lower the required impedances will be. When the real part is several orders of magnitude lower than the imaginary part, the solutions are close to the fringe cases of $\infty\,\Omega$ and $0\,\Omega$, shown in Equations (15) and (17).

## 3. MEASUREMENTS

### 3.1. Complex Impedance Transformer

The design process was used to design a $3\,\mathrm{dB}$ $90°$ balanced hybrid with a $50\,\Omega$ to $70 - 200j\,\Omega$ transformation (i.e., $Z_0 = 50\,\Omega$ and $Z_T = 70 - 200j\,\Omega$) at $2\,\mathrm{GHz}$ on a $30\,\mathrm{mil}$ thick Arlon 25N substrate. The renormalized $S$ parameters with ideal transmission lines are shown in Figs. 2 and 3.

Afterwards, the circuit was optimized taking into account discontinuities and T-junctions using the full-wave simulator HFSS with the goal of behaving as similar as possible to the ideal case, which fall relatively close to the originals, as seen in Table 4.

The manufactured circuit, shown in Fig. 4, covers an area of $66.1 \times 33.9\,\mathrm{mm}^2$. Its $S$ parameters were measured with a $50\,\Omega$ vector network analyzer, which were then renormalized to $70 - 200j\,\Omega$ in ports 3 and 4 using equations from [17], depicted in Figs. 5–8. Due to its symmetry and reciprocity, only the relevant $S$ parameters are shown.
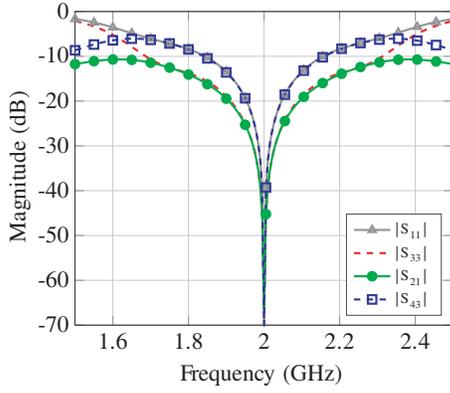
**Figure 2.** Matching and isolation of the $50\,\Omega$ to $70-200j\,\Omega$ hybrid coupler with ideal transmission lines.
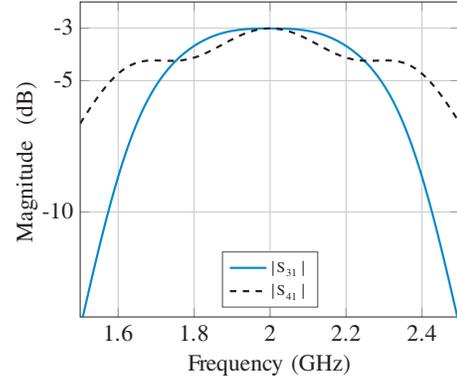
**Figure 3.** Insertion loss of the $50\,\Omega$ to $70-200j\,\Omega$ hybrid coupler with ideal transmission lines.

**Table 4.** Initial and final values for impedances and lengths of the $50\,\Omega$ to $70-200j\,\Omega$ hybrid coupler.

|         | $Z_1$        | $Z_2$         | $Z_{B1}$      | $Z_{B2}$    | $Z_A$        | $L_1$       | $L_2$        |
|---------|--------------|---------------|---------------|-------------|--------------|-------------|--------------|
| Initial | $78.4\,\Omega$ | $127.4\,\Omega$ | $123.1\,\Omega$ | $19\,\Omega$  | $34.2\,\Omega$ | $90°$       | $59.7°$      |
| Final   | $78.5\,\Omega$ | $128.2\,\Omega$ | $123\,\Omega$   | $19\,\Omega$  | $34.2\,\Omega$ | $90°$       | $56°$        |
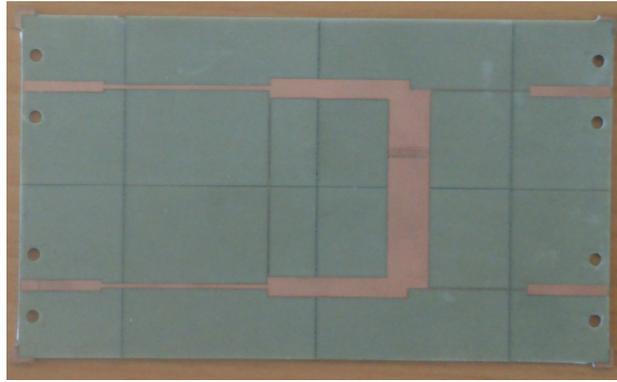


**Figure 4.** Measured $3\,\mathrm{dB}$ $90°$ balanced hybrid with a $50$ to $70-200j\,\Omega$ transformation. $50\,\Omega$ lines were added to each port for TRL calibration.

There is a very good agreement between simulations and measurements. The hybrid presents matching and isolation between adjacent ports above $20\,\mathrm{dB}$ at $2\,\mathrm{GHz}$. The matching above $10\,\mathrm{dB}$ at ports 1 and 2 is the most limiting factor in bandwidth, resulting in a roughly $14.75\%$ bandwidth centered on $2\,\mathrm{GHz}$, yielding an amplitude balance of $3.85 \pm 0.85\,\mathrm{dB}$ and a phase balance of $90.12° \pm 3.64°$.

### 3.2. Real Impedance Matching

To compare to the impedance-transforming hybrid couplers of [10], a $50\,\Omega$ to $450\,\Omega$ hybrid coupler was designed and manufactured. The transforming ratio of $450\,\Omega$ to $50\,\Omega$ is bigger than any of the impedance-transforming hybrids found in the literature. As before, a $3\,\mathrm{dB}$ $90°$ balanced hybrid at $2\,\mathrm{GHz}$ on a $30\,\mathrm{mil}$ thick Arlon 25N substrate was designed and manufactured, shown in Fig. 9. It covers an area of $71 \times 31.5\,\mathrm{mm}^2$. The final impedances are $Z_1 = 64.3\,\Omega$, $Z_{B1} = 132.43\,\Omega$, $Z_A = 35.7\,\Omega$, $Z_{B2} = 25\,\Omega$ and $Z_2 = 90.36\,\Omega$, with the line lengths of $90°$.
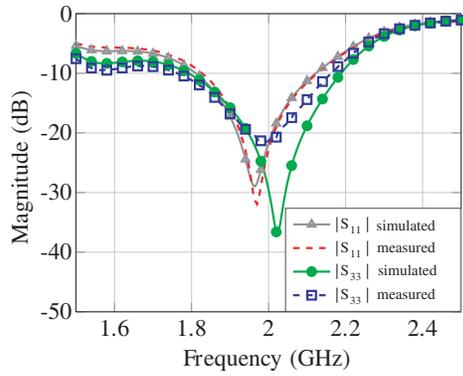
**Figure 5.** Matching of the measured $50\,\Omega$ to $70 - 200j\,\Omega$ hybrid coupler.
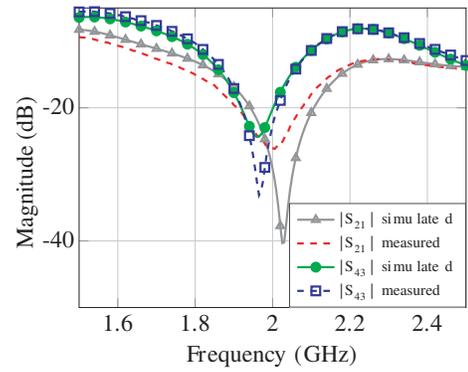


**Figure 6.** Isolation between adjacent ports of the measured $50\,\Omega$ to $70 - 200j\,\Omega$ hybrid coupler.
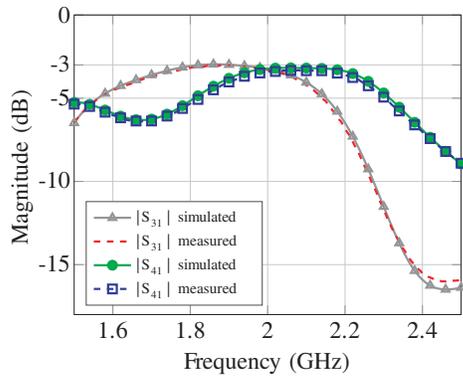


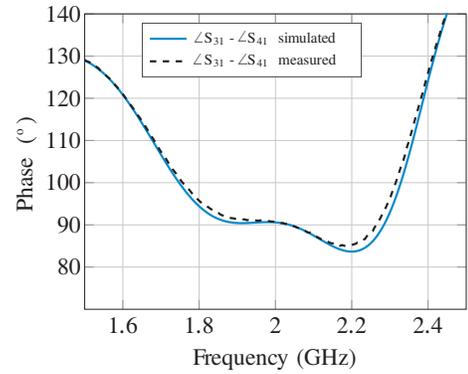**Figure 7.** Insertion loss of the measured $50\,\Omega$ to $70 - 200j\,\Omega$ hybrid coupler.



**Figure 8.** Phase difference between the direct and coupled ports of measured the $50\,\Omega$ to $70 - 200j\,\Omega$ hybrid coupler.
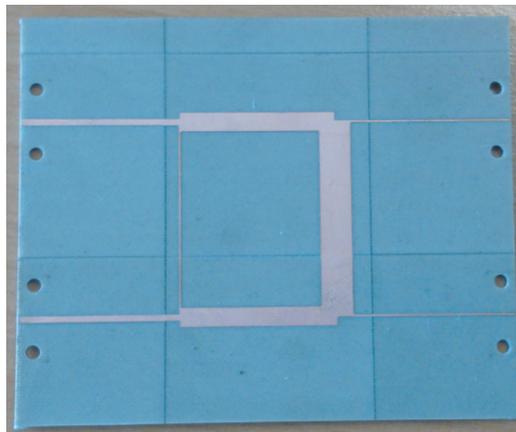


**Figure 9.** Measured $3\,\text{dB}$ $90°$ balanced hybrid with a $50\,\Omega$ to $450\,\Omega$ transformation.

Observing the $S$ parameters shown in Figs. 10–13, the hybrid presents matching above $20\,\text{dB}$ and isolation between ports above $15\,\text{dB}$ at $2\,\text{GHz}$. The matching at ports 1 and 2 is the most limiting factor in bandwidth, resulting in a roughly $21\%$ bandwidth centered on $2\,\text{GHz}$, yielding an amplitude balance of $4.35 \pm 1\,\text{dB}$ and a phase balance of $92.16° \pm 8.8°$. Although the amplitude balance is higher than in
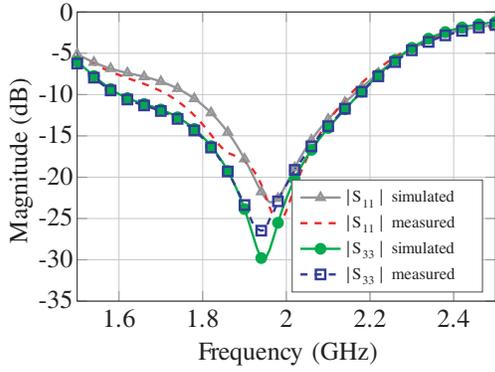
**Figure 10.** Matching of the measured $50\,\Omega$ to $450\,\Omega$ hybrid coupler.
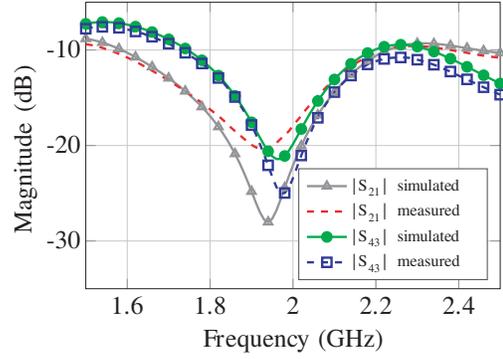


**Figure 11.** Isolation between adjacent ports of the measured $50\,\Omega$ to $450\,\Omega$ hybrid coupler.
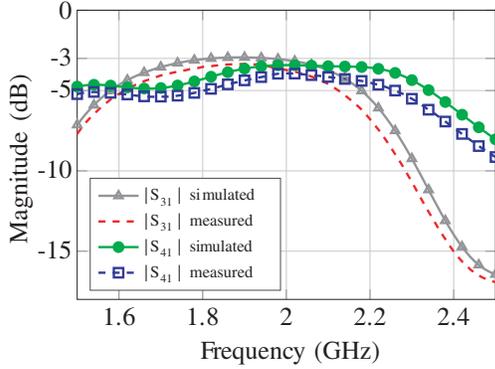


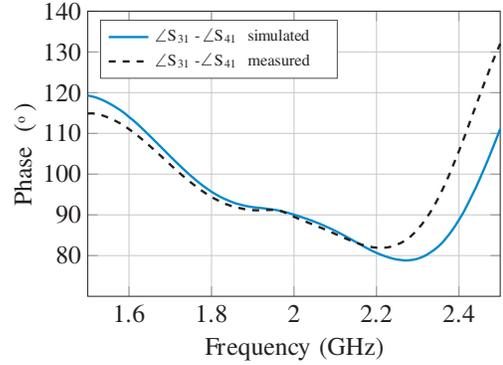**Figure 12.** Insertion loss of the measured $50\,\Omega$ to $450\,\Omega$ hybrid coupler.



**Figure 13.** Phase difference between the direct and coupled ports of measured the $50\,\Omega$ to $450\,\Omega$ hybrid coupler.

other couplers, it is due to the high transforming ratio [18]. Nonetheless, the behaviour is equal to that of a hybrid transforming to a lesser impedance.

### 3.3. Line Length Reduction

When matching to a real impedance, the shortest transforming line length needed is of $90°$. If size were an issue, reducing its length could be achievable by matching to a complex impedance that would still yield a good enough matching. Generally, a matching above $10\,\mathrm{dB}$ can be considered a good compromise between line length and matching. Applying it to $Z_0$, it would mean matching the first and second ports to a complex impedance, whose real part is $Z_0$. In order to demonstrate this, the same $50\,\Omega$ to $70 - 200j\,\Omega$ hybrid coupler was designed again, but with ports 1 and 2 matched to $50 - 20j\,\Omega$, which should produce a matching around $15\,\mathrm{dB}$. The renormalized $S$ parameters are shown in Figs. 14 and 15. As expected, they are similar to those in Figs. 2 and 3, but with lower matching for every port.

**Table 5.** Initial and final values for impedances and lengths of the reduced $50\,\Omega$ to $70 - 200j\,\Omega$ hybrid coupler.

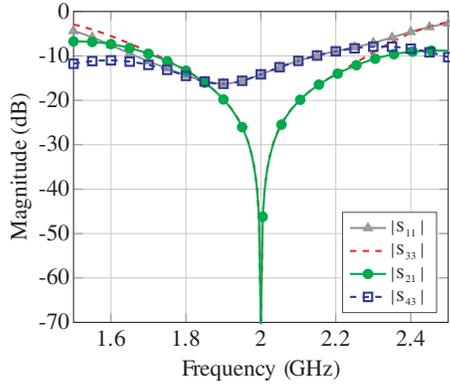|  | $Z_1$ | $Z_2$ | $Z_{B1}$ | $Z_{B2}$ | $Z_A$ | $L_1$ | $L_2$ |
|---|---|---|---|---|---|---|---|
| Initial | $38\,\Omega$ | $127\,\Omega$ | $64.5\,\Omega$ | $19\,\Omega$ | $24.7\,\Omega$ | $23.1°$ | $59.7°$ |
| Final | $47.5\,\Omega$ | $118.1\,\Omega$ | $64.6\,\Omega$ | $19\,\Omega$ | $24.7\,\Omega$ | $18.8°$ | $60°$ |

**Figure 14.** Matching and isolation of the reduced $50\,\Omega$ to $70 - 200j\,\Omega$ hybrid coupler with ideal transmission lines.
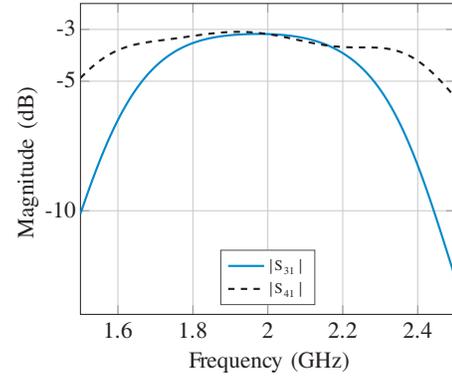


**Figure 15.** Insertion loss of the reduced $50\,\Omega$ to $70 - 200j\,\Omega$ hybrid coupler with ideal transmission lines.
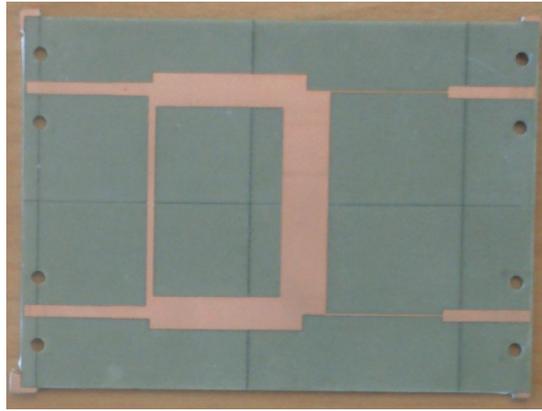


**Figure 16.** Measured, reduced $3\,\text{dB}$ $90°$ balanced hybrid with a $50\,\Omega$ to $70 - 200j\,\Omega$ transformation. $50\,\Omega$ lines were added to each port for TRL calibration.



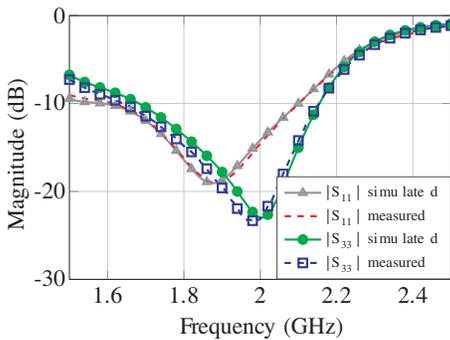**Figure 17.** Matching of the measured, reduced $50\,\Omega$ to $70 - 200j\,\Omega$ hybrid coupler.
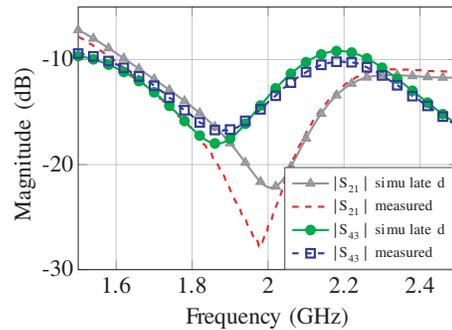


**Figure 18.** Isolation between adjacent ports of the measured, reduced $50\,\Omega$ to $70 - 200j\,\Omega$ hybrid coupler.

The impedance and line length values were again optimized through HFSS, obtaining values similar to the initial ones, as shown in Table 5. The manufactured circuit, shown in Fig. 16, covers an area of $46.8 \times 35.9\,\text{mm}^2$, which constitutes a 25% reduction of the previous circuit. Its $S$ parameters are depicted in Figs. 17–20.
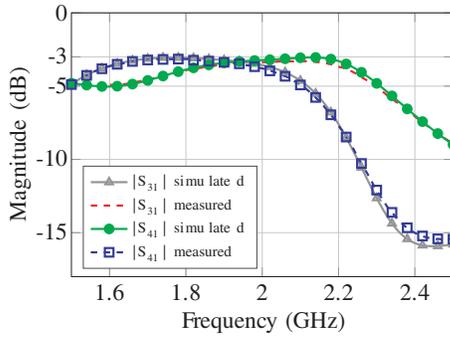
**Figure 19.** Insertion loss of the measured, reduced $50\,\Omega$ to $70 - 200j\,\Omega$ hybrid coupler.
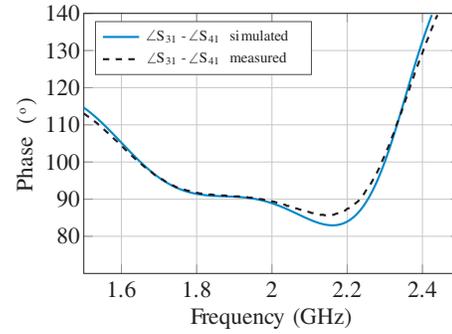


**Figure 20.** Phase difference between the direct and coupled ports of the measured, reduced $50\,\Omega$ to $70 - 200j\,\Omega$ hybrid coupler.

There is still good agreement between measurements and simulations. While the matching in ports 1 and 2 is now below 20 dB, it is worth noting that the bandwidth has increased to 22.5%. The amplitude balance is $4 \pm 0.9$ dB and the phase balance is $93.22° \pm 6.74°$. While slightly worse than before, this is due to the bandwidth increase.

This technique could have also been used to reduce the line length when transforming to real impendances, as it could apply to the lines in both ports, decreasing the 90° electrical length.

## 4. CONCLUSION

A modified topology of the impedance-transforming hybrid coupler is presented, which allows the increase in the impedance transforming ratio of real impedances and, more importantly, permits matching complex impedances. An even-odd analysis was realized, obtaining design equations and detailing the design process to realize the desire impedance-transforming hybrid coupler. Sample cases were discussed to show the impedance limitations, which are more restrictive when matching to complex impedance with a higher imaginary to real part ratio.

A $50\,\Omega$ to $450\,\Omega$ hybrid coupler was manufactured to demonstrate how the high transforming ratio of real impedances has little effect on the desired behaviour when compared to other hybrids in the literature. Bandwidth, amplitude and phase balance are within expected values.

Two $50\,\Omega$ to $70 - 200j\,\Omega$ hybrid couplers were designed and manufactured. Both show that the design process produces values that don't differ much to those obtained after being optimized through a full-wave simulator. One of those transformers also show that a significant reduction of chip size can be made by shortening the length of the transmission line that matches a real impedance, and thus matching to a complex impedance that still gives a reasonable matching. That reduction is shown to not have any negative impact on the performance of the hybrid. On the contrary, the bandwidth is increased.

## REFERENCES

1. Wang, Q., J. Lim, and Y. Jeong, "Design of a compact dual-band branch line coupler using composite right/left-handed transmission lines," *Electronics Letters*, Vol. 52, No. 8, 630–631, April 2016.

2. Kim, H., H. Wi, S. Wang, J. Kim, and W. Jung, "'Broadband 3 dB microstrip hybrid coupler with low dielectric substrate for X-Band applications," *2016 IEEE 17th Annual Wireless and Microwave Technology Conference (WAMICON)*, 1–3, Clearwater, FL, 2016.

3. Morimoto, Y., A. Waghmare, K. Dhwaj, and T. Itho, "A compact branch line coupler using novel periodically grounded slow-wave structure," *2016 IEEE MTT-S International Microwave Symposium (IMS)*, 1–3, San Francisco, CA, 2016.

4. Hettak, K. and K. Elgaid, "3D Ultra miniature MMIC TFMS 90° coupler fabricated with a standard air bridge process," *2011 41st European Microwave Conference (EuMC)*, 846–849, Manchester, 2011.

5. Nosrati, M., "An extremely miniaturized microstrip branch-line coupler," *MicroWave and Optical Technology Letters*, Vol. 51, No. 6, 1403–1406, June 2009.

6. Cheng, S., E. Ojefors, P. Hallbjorner, and A. Rydberg, "Compact reflective microstrip phase shifter for traveling wave antenna applications," *IEEE Microwave and Wireless Components Letters*, Vol. 16, No. 7, 431–433, July 2016.

7. Wong, Y. S., S. Y. Zheng, and W. S. Chan, "Multifolded bandwidth branch line coupler with filtering characteristic using coupled port feeding," *Progress In Electromagnetics Research*, Vol. 118, 17–35, 2011.

8. Cheng, Y. J., L. Wang, J. Wu, and Y. Fan, "Directional coupler with good restraint outside the passband and its frequency-agile application," *Progress In Electromagnetics Research*, Vol. 135, 759–771, 2013.

9. Gai, C., Y. C. Jiao, and Y. L. Zhao, "Compact dual-band branch-line coupler with dual transmission lines," *IEEE Microwave and Wireless Components Letters*, Vol. 26, No. 5, 325–327, May 2016.

10. Gupta, R., S. Anderson, and W. Getsingert, "Impedance-transforming 3-dB 90° hybrids," *IEEE Transactions on Microwave Theory and Techniques*, Vol. 35, No. 12, 1303–1307, December 1987.

11. Lin, C.-S., S.-F. Chang, C.-C. Chang, and Y.-H. Shu, "Design of a reflection-type phase shifter with wide relative phase shift and constant insertion loss," *IEEE Transactions on Microwave Theory and Techniques*, Vol. 55, No. 9, 1862–1868, September 2007

12. Jing, X. and S. Sun, "Design of impedance transforming 90 degree patch hybrid couplers," *2014 Asia-Pacific Microwave Conference (APMC)*, 25–27, Nov. 4–7, 2014.

13. Kumar, S., C. Tannous, and T. Danshin, "A multisection broadband impedance transforming branch-line hybrid," *IEEE Transactions on Microwave Theory and Techniques*, Vol. 43, No. 11, 2517–2523, Nov. 1995.

14. Alcón, P., N. Esparza, L. F. Herrán, and F. Las Heras, "On the design of generic matching networks in reflective-type phase shifters for antennas," *2015 9th European Conference on Antennas and Propagation (EuCAP)*, 1–5, Lisbon, 2015.

15. Hee-Ran, A., "Complex impedance transformers consisting of only transmission-line sections," *IEEE Transactions on Microwave Theory and Techniques*, Vol. 60, No. 7, 2073–2083, July 2012.

16. Reed, J. and G. J. Wheeler, "A method of analysis of symmetrical four-port networks," *IRE Transactions on Microwave Theory and Techniques*, Vol. 4, No. 4, 246–252, October 1956.

17. Kurokawa, K., "Power waves and the scattering matrix," *IEEE Transactions on Microwave Theory and Techniques*, Vol. 13, No. 2, 194–202, March 1965.

18. Lind, L. F., "Synthesis of asymmetrical branch-guide directional coupler-impedance transformers (correspondence)," *IEEE Transactions on Microwave Theory and Techniques*, Vol. 17, No. 1, 45–48, January 1969.